



# Using texture analysis to improve per-pixel classification of very high resolution images for mapping plastic greenhouses

Francisco Agüera\*, Fernando J. Aguilar, Manuel A. Aguilar

*Departamento de Ingeniería Rural, Universidad de Almería, 04120, Spain*

Received 10 January 2007; received in revised form 26 March 2008; accepted 28 March 2008

Available online 6 May 2008

## Abstract

The area occupied by plastic-covered greenhouses has undergone rapid growth in recent years, currently exceeding 500,000 ha worldwide. Due to the vast amount of input (water, fertilisers, fuel, etc.) required, and output of different agricultural wastes (vegetable, plastic, chemical, etc.), the environmental impact of this type of production system can be serious if not accompanied by sound and sustainable territorial planning. For this, the new generation of satellites which provide very high resolution imagery, such as QuickBird and IKONOS can be useful. In this study, one QuickBird and one IKONOS satellite image have been used to cover the same area under similar circumstances. The aim of this work was an exhaustive comparison of QuickBird vs. IKONOS images in land-cover detection. In terms of plastic greenhouse mapping, comparative tests were designed and implemented, each with separate objectives. Firstly, the Maximum Likelihood Classification (MLC) was applied using five different approaches combining R, G, B, NIR, and panchromatic bands. The combinations of the bands used, significantly influenced some of the indexes used to classify quality in this work. Furthermore, the quality classification of the QuickBird image was higher in all cases than that of the IKONOS image. Secondly, texture features derived from the panchromatic images at different window sizes and with different grey levels were added as a fifth band to the R, G, B, NIR images to carry out the MLC. The inclusion of texture information in the classification did not improve the classification quality. For classifications with texture information, the best accuracies were found in both images for mean and angular second moment texture parameters. The optimum window size in these texture parameters was  $3 \times 3$  for IK images, while for QB images it depended on the quality index studied, but the optimum window size was around  $15 \times 15$ . With regard to the grey level, the optimum was 128. Thus, the optimum texture parameter depended on the main objective of the image classification. If the main classification goal is to minimize the number of pixels wrongly classified, the mean texture parameter should be used, whereas if the main classification goal is to minimize the unclassified pixels the angular second moment texture parameter should be used. On the whole, both QuickBird and IKONOS images offered promising results in classifying plastic greenhouses.

© 2008 International Society for Photogrammetry and Remote Sensing, Inc. (ISPRS). Published by Elsevier B.V. All rights reserved.

**Keywords:** QuickBird; IKONOS; Texture; Land use

## 1. Introduction

Plastic-covered greenhouses have undergone rapid expansion in recent years, covering over 500,000 ha

worldwide. The largest concentrations are in Asia (China with 20,000 ha, Korea with 27,000 ha, and Japan with 70,000 ha), followed by the Mediterranean basin (currently with over 130,000 ha). In the Americas, this trend has also been followed. Due to the high cost effectiveness of this production system, greenhouse agriculture

\* Corresponding author.

E-mail address: [faguera@ual.es](mailto:faguera@ual.es) (F. Agüera).

strongly influences the economy of the area where it is implemented, in some cases representing practically the only source of income. This is the case at the Almería coast, in south-eastern Spain, with an annual production of approximately  $3 \times 10^9$  kg of produce at an approximate value of  $1900 \times 10^9$  Euros. As a consequence of the rapid expansion of the greenhouse surface area, with almost no planning in some of these areas, a number of environmental problems have arisen and are becoming more serious as this surface area keeps growing: the generation and accumulation of vegetable and plastic waste, over-exploitation of water resources in the area, encroachment on protected natural areas, the absence of a road network to cover the needs of existing transport, etc. These factors render the production system unsustainable and endanger the local economy (Parra, 2004). In order to alleviate these problems and to find solutions for the future, different organisations are seeking to establish methods to calculate as accurately as possible the surface area occupied by greenhouses.

In Spain, Sanjuán (2004) carried out a study using Thematic Mapper images from the Landsat 5 and 7 satellites in order to estimate the greenhouse surface area in south-eastern Spain. The problems of the imagery from these satellites to detect greenhouses are similar to those that appear when working in urban areas: few greenhouse pixels are thematically pure, and land use must be inferred from image characteristics or through the incorporation of ancillary information (Guindon et al., 2004). Consequently, aerial orthophotographs are used when working in areas with this type of land use. The arrival of new satellites that provide Very High Resolution (VHR) imagery, such as IKONOS (IK) and QuickBird (QB), has opened new ways of tackling this problem, as they can detect small objects. Although the use of imagery from IK or QB is widespread in urban areas, this is not the case in greenhouse areas. Besides the study by Sanjuán (2004) mentioned above, Agüera et al. (2006) also used a QB image to examine the evolution of the surface area occupied by greenhouses in a zone of south-eastern Spain. These VHR images had already been used for detecting buildings (Fraser et al., 2002; Weber and Ranchin, 2003; Mesev, 2005), roads (Yan and Zhao, 2003; Jin and Davis, 2005), vegetation (Nichol and Lee, 2005), and even buildings damaged by various disasters (Al-Khudhairy et al., 2005). For greenhouse detection by satellite imagery, a series of considerations must be taken into account due to the construction material used and its handling: the spectral signature of plastic changes drastically depending on the vision angle, chemical composition and even age of the plastic.



Fig. 1. Study site images from QuickBird (above) and IKONOS (below).

Moreover, in some areas at certain times of the year the plastic sheets are painted white to avoid excessive light and heat inside the greenhouse. At other times of the year, the plastic is not painted, and this changes its response to the band of the infrared spectrum. Also, different types of plastic are used in the same greenhouse, due to partial replacements, (repair of tears), and even materials other than plastic (i.e. the mesh covering the opening for roof ventilation) are used. All these factors trigger widely different spectral responses from one greenhouse to another, even within the same greenhouse, making it difficult to propose a specific image-classification technique for detection. Fig. 1 presents images from QB and IK for the study site, showing the heterogeneity of plastic spectral signature.

Most of the imagery classification methods are based on the statistical analysis of each separate pixel. These methods have shown good performance when used for images with a relatively large pixel size (Wang et al., 2004). In VHR imagery, with smaller pixel size, the detectable spectral variability may increase within a particular class, making the classification process even harder (Cushnie, 1987; Shaban and Dikshit, 2001), especially in the case of anthropogenic structures (Kiema, 2002). To avoid this problem as much as possible, different techniques have been developed that take into account both the spectral information and the information supplied by the texture of the image. These techniques have been used mainly in urban

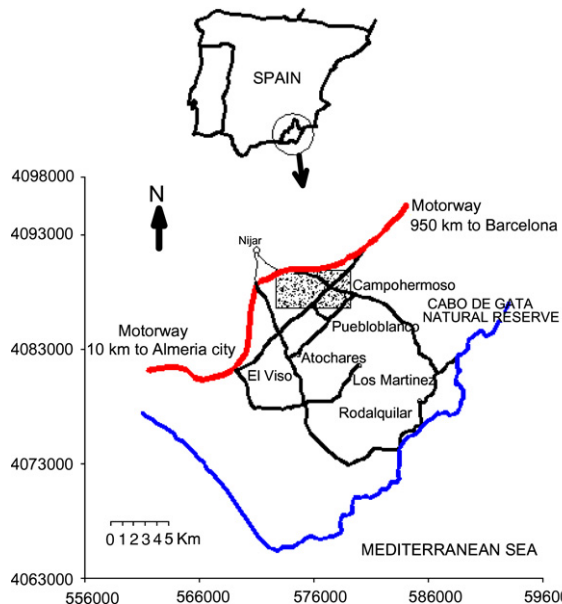


Fig. 2. Location of the study area (shadow rectangle), where main villages and roads have been located. Coordinates are UTM (zone 30, ED50).

areas. The output image generated by texture analysis is often classified directly or used as an additional band together with other multi-spectral bands in the classification procedure (Lee et al., 2003; Wang et al., 2004; Puissant et al., 2005). The information regarding the texture of the image has also been used by different authors to establish parameters related to the area under study. Kayitakire et al. (2006), deduced forest-structure variables (age, top height, circumference and basal area) from image-texture analysis and IKONOS-2 imagery. Other authors, such as Franklin et al. (2001) and Rao et al. (2002), have used the textural information from satellite images for land-use classification in forest areas.

The aim of the present study is to perform an exhaustive comparison of QuickBird vs. IKONOS images in terms of their accuracy in classifying land use. Focusing on plastic-greenhouse mapping, we designed and implemented two comparison tests, each with separate objectives. Firstly, to study the accuracy of spectral bands for classifying land use, we made the Maximum Likelihood Classification (MLC) using five different approaches combining R, G, B, NIR, and panchromatic bands. Secondly, to study the usefulness of texture information in land-use classification, we derived texture features from the panchromatic images at different window sizes and with different grey-level quantification, and these were added as a fifth band to the R, G, B, NIR image to carry out the MLC.

## 2. Study site and data preparation

### 2.1. Study site

The area selected is situated in the east of the Almería province (south-eastern Spain, Fig. 2). This is currently the most dynamic zone in the province in terms of greenhouse spreading, with approximately 6000 ha concentrated in an area of 18 000 ha. However it has low-quality water resources and shares a boundary with the Cabo de Gata Natural Reserve, a spot of great ecological wealth that is threatened by over-exploitation of resources, and the activity derived from the vast greenhouse overcrowding nearby (residues, sewage, etc.). For our study we chose a rectangle of 2084.27 ha ( $6425 \times 3244$  m), with UTM coordinates (zone 30, ED-50) of the SW and NE vertexes (572740, 4086640) and (579165, 4089884), respectively.

### 2.2. Data preparation

In this study, we used two images, one from QB and one from IK satellites. On 19 December 2004 a QB basic image by DigitalGlobe was acquired. The basic scene was centred on coordinates WGS-84 (latitude and longitude) of  $36.93045^\circ$  N and  $2.12685^\circ$  W. The QB basic product consisted of one panchromatic image and one multi-spectral image collecting data on blue, green, red, and near-infrared wavelengths (B, G, R, NIR). Data for each band were stored with 11-bit quantification. Basic imagery products were radiometrically and sensor corrected, but not geometrically corrected or mapped to a cartographic projection and ellipsoid. They are accompanied by information related to satellite attitude, ephemeris, and camera model information. Multi-spectral and panchromatic imagery were orthorectified with a resolution of 2.5 and 0.61 m, respectively (for details of this process, see Aguilar et al. (2005)). In September 2005, an archive image of the IK Geo Ortho Kit, taken on 2 June 2005 was acquired from European Space Imaging. Similarly to the QB imagery, this product consisted of one panchromatic image and one multi-spectral image (B, R, G, NIR), recorded in 11 bits. Multi-spectral and panchromatic imagery was orthorectified with a resolution of 4 and 1 m, respectively.

To quantify the accuracy of the results of the classification processes implemented, we manually delineated the greenhouses from panchromatic QB and IK orthoimages, as well as field data. A total greenhouse surface area of 708.86 and 715.96 ha, respectively, was quantified from these images.

Table 1

Average number of pixels and standard deviation (in brackets), used in the five replications of training areas for each image

Image	Pixels in sub-class 1 (SD)	Pixels in sub-class 2 (SD)	Pixels in sub-class 3 (SD)
QuickBird ( $2.5 \times 2.5$ m)	4160 (131)	6610 (1078)	4094 (655)
IKONOS ( $4 \times 4$ m)	8997 (1687)	20 755 (2270)	12 670 (2920)

### 3. Methods

#### 3.1. Classification based on spectral information

The MLC method was chosen to help compare the performance of the two different satellite-image sources. Several studies have successfully used this classification method, either alone or in combination with other methods (e.g. Gong et al. (1992), Green et al. (1998), Gao (1999), Lee et al. (2003), Wang et al. (2004), Puissant et al. (2005) and Agüera et al. (2006)).

The aim of this classification was to portray the areas occupied by greenhouses in both images as accurately as possible. The study of the images showed high variability in the reflectance of greenhouses. Therefore, they were divided into three sub-classes with more homogeneous spectral signatures in the RGB combination bands. This is based on previous work (Agüera et al., 2006) showing that three sub-classes are sufficient to identify significant differences between spectral clusters of greenhouses and other buildings. Once the training sites had been defined, the MLC was implemented using two different approaches. In the first, only the multi-spectral bands were fed into the MLC, and the results from this test provided a comparison performance using only the multi-spectral bands of the images. In the second approach, the panchromatic band was taken into account and added to the classification process together with the multi-spectral bands. For this classification test, panchromatic images of QB and IK were re-sampled at 2.5 and 4 m, respectively, and added to their multi-spectral image, resulting in two five-channel images at a spatial resolution of 2.5 and 4 m. The results from this option were used to compare the contribution of the panchromatic band to the accuracy of the classification in both images.

For each image, five replications were made, taking into account five different sets of training sites, which were used for both types of classification. Table 1 shows the average number of training pixels for each sub-class and image. In each case, the number of training pixels varied between 0.22 and 0.71% of the total of the study area, which can be considered sufficient for a correct classification (Lee et al., 2003; Van Niel et al.,

2005). PCI Geomatica V9.1 software was used for these classifications.

#### 3.2. Classification with the inclusion of texture information

Texture is the visual effect caused by spatial variation in tonal quantity over relatively small areas (Any and He, 1995). In the literature, the main approach to texture analysis is based on the Grey Level Co-occurrence Matrix (GLCM) method (Haralick et al., 1973), although other approaches based on variograms, fractal dimension, or neural networks can be found. Most of the texture measures are computed from GLCM directly. In addition, some texture measures are computed from a Grey-Level-Difference Vector (GLDV), which itself is derived from a GLCM.

In the present study, the methodology applied uses the re-sampled panchromatic band to derive textural information. The output image generated by texture analysis is then added to the four multi-spectral bands (R, G, B, NIR). The five-band image is then classified using the MLC method and the result is a spectral/textural classification (Puissant et al., 2005). The co-occurrence matrix values were calculated with seven window sizes (ws) ( $3 \times 3$ ,  $5 \times 5$ ,  $7 \times 7$ ,  $9 \times 9$ ,  $11 \times 11$ ,  $15 \times 15$ ,  $21 \times 21$ ), and the grey level with six values (1024, 256, 128, 64, 32, 16). Displacement vectors in four directions ( $0^\circ$ ,  $45^\circ$ ,  $90^\circ$ ,  $135^\circ$ ) with a spatial distance of 1 pixel were used to produce the average value of each texture measure.

Ten texture measures were used:

– Homogeneity:

$$\text{HOM} = \sum_{i=0}^{N-1} \sum_{j=0}^{N-1} \frac{P(i, j)}{1 + (i - j)^2}. \quad (1)$$

– Contrast:

$$\text{CON} = \sum_{i=0}^{N-1} \sum_{j=0}^{N-1} P(i, j) \times (i - j)^2. \quad (2)$$

– Dissimilarity:

$$\text{DIS} = \sum_{i=0}^{N-1} \sum_{j=0}^{N-1} P(i, j) \times |i - j|. \quad (3)$$

– Mean:

$$\text{MEA}_i = \sum_{i=0}^{N-1} \sum_{j=0}^{N-1} i \times P(i, j). \quad (4)$$

– Standard deviation:

$$\text{STD}_i = \left[ \sum_{i=0}^{N-1} \sum_{j=0}^{N-1} P(i, j) \times (i - \text{MEA}_i)^2 \right]^{1/2}. \quad (5)$$

– Entropy:

$$\text{ENT} = \sum_{i=0}^{N-1} \sum_{j=0}^{N-1} -P(i, j) \times \log_e(P(i, j)). \quad (6)$$

– Angular second moment:

$$\text{ASM} = \sum_{i=0}^{N-1} \sum_{j=0}^{N-1} P(i, j)^2. \quad (7)$$

– Correlation:

$$\text{COR} = \sum_{i=0}^{N-1} \sum_{j=0}^{N-1} \frac{P(i, j) \times (i - \text{MEA}_i) \times (j - \text{MEA}_j)}{\text{STD}_i \times \text{STD}_j}. \quad (8)$$

– GLDV angular second moment:

$$G\text{-ASM} = \sum_{k=0}^{N-1} V(k)^2. \quad (9)$$

– GLDV entropy:

$$G\text{-ENT} = \sum_{k=0}^{N-1} (-V(k)) \times \log_e(V(k)) \quad (10)$$

where  $N$  is the number of grey levels,  $P$  is the normalised symmetric GLCM of dimension  $N \times N$ ;  $V$  is the normalised grey-level-difference vector of dimension  $N$ ;  $P(i, j)$  is the normalised co-occurrence matrix such that  $\sum_{i=0}^{N-1} \sum_{j=0}^{N-1} P(i, j) = 1$ , and  $V(k)$  is the normalised grey level-difference vector:  $\sum_{i=0}^{N-1} \sum_{j=0}^{N-1} P(i, j)$ , with  $|i - j| = k$ .

All these combinations of ws, grey levels, and texture measures give a total of  $6 \times 7 \times 10 = 420$  different classifications per image. For each classification, five replications were carried out taking into account the five different sets of training areas described in Table 1. The texture measures were made with PCI Geomatica V9.1 software, but to automate the classification of all these 420 treatments  $\times$  5 replications  $\times$  2 images (4200) cases, an application developed by the authors in Visual Basic 6.0 programming language was used. For input, it took the multi-spectral bands, the texture measures and the

training areas, and for output gave the pixels classified as greenhouse.

### 3.3. Performance evaluation for greenhouse extraction

The quality of the greenhouse extraction process was assessed from the indexes defined by McKeown (1999). The greenhouses automatically detected were compared pixel by pixel with those manually delineated ones (true classification). The results for each pixel in the image fell into one of four categories:

- (1) True positive (TP): both the automated and manual methods label a pixel as greenhouse.
- (2) True negative (TN): both the automated and manual methods label a pixel as background (non-greenhouse).
- (3) False positive (FP): only the automated method labels a pixel as greenhouse.
- (4) False negative (FN): only the manual method labels a pixel as greenhouse.

Using these four categories, the following summary statistics were computed:

- (1) Branching factor (BF):  $FP/TP$ .
- (2) Miss factor (MF):  $FN/TP$ .
- (3) Greenhouse detection percentage (GDP):  $100 \text{ TP}/(\text{TP} + \text{FN})$ .
- (4) Quality percentage (QP):  $100 \text{ TP}/(\text{TP} + \text{FP} + \text{FN})$ .

The branching factor provides an incorrect pixel fraction labelling them as greenhouses, while the miss factor indicates the ratio of pixels not classified as greenhouses, despite actually being greenhouses. These two factors are calculated with regard to the pixels correctly classified as greenhouses (TP), and describe the two types of possible errors that can appear in the classification process. The greenhouse detection percentage is the percentage of greenhouse pixels correctly detected by the automatic process. The quality percentage indicates the likelihood of a pixel being correctly classified. In the classification process, the aim should be to reduce the two types of possible errors: FP and FN. The statistics described above were calculated for each repetition in the different treatments.

To determine whether the treatments of the classification based on spectral information significantly influenced the outcome of the classification, several two-way ANOVA tests were applied (Steel and Torrie, 1980), in which the dependent variable was one of the different statistics described above, while the factors consisted of the images and the various band combinations used to carry out the MLC. Furthermore, to determine whether

Table 2

ANOVA tables of the significance of the two factors (treatment: bands used to carry out the classification, and image: image from QuickBird and IKONOS), and their interactions on quality classification indexes (df: degree of freedom)

Source	df	Sum of squares	F-values	P-values
<b>BF</b>				
Image (A)	1	0.24366	15.1	<0.001
Treat. (B)	3	0.08981	1.85	0.1572
A*B	3	0.0043	0.09	0.9657
Residual	32	0.51652		
Total	39	0.85427		
<b>MF</b>				
Image (A)	1	0.00119	3.24	0.0811
Treat. (B)	3	0.06801	61.67	<0.001
A*B	3	1.46E−04	0.13	0.9401
Residual	32	0.01176		
Total	39	0.08112		
<b>GDP</b>				
Image (A)	1	7.76717	3.3	0.0788
Treat. (B)	3	469.933	66.46	<0.001
A*B	3	0.91645	0.13	0.9418
Residual	32	75.4181		
Total	39	554.035		
<b>QP</b>				
Image (A)	1	758.871	23.31	<0.001
Treat. (B)	3	31.5435	0.32	0.8087
A*B	3	14.8972	0.15	0.9273
Residual	32	1041.95		
Total	39	1847.26		

the texture parameters significantly affected the outcome of the classification, several multi-way ANOVA tests were made in which the dependent variable was one of the different statistics described above, whereas the factors consisted of the two different images, the texture parameter, ws, and grey level.

## 4. Results and discussion

### 4.1. Comparison of the classification based on spectral information

Table 2 presents the ANOVA results of the significance of the two factors (bands used to carry out the classification, and image type), and their

interactions on quality classification indexes described in Section 3.3. Table 3 lists the average values of the quality indexes obtained from the classification carried out with the spectral information from each of the images studied. Table 2 indicates that factor A (image) was significant to explain only the overall variation of BF and QP indexes, and in both cases mean differences for this factor were found significant using the LSD test ( $p < 0.05$ ), showing the significant higher indexes in the QB image (Table 3). Factor B (bands used to carry out the classification) was significant to explain the overall variation of MF and GDP (Table 2). The LSD test indicated that treatment 1 (RGB bands to carry out the classification) gave the best indexes, as reflected in Table 3 (0.032 and 0.040 for MF, and 96.89 and 96.12 for GDP, in QB and IK respectively). Factor B did not explain the overall variation of BF and QP, signifying that the fraction of pixels incorrectly labelled as greenhouses did not significantly improve when different band combinations were used. Agüera et al. (2006), also working with greenhouses, found no differences in the BF, either, when using different multi-spectral band combinations to define the training areas and to carry out a MLC classification of a QB image. That work showed a similar tendency of MF as in our work: a significantly higher MF when the classification was made by adding NIR than when using only RGB bands (treatment 1). This behaviour of MF could be explained by taking into account that training areas were defined from image with RGB bands, and the addition of a new band to carry out the classification could interfere negatively in the classification accuracy. We can see in Table 3 that MF and GDP tended to become worse when bands other than RGB were added to carry out the MLC. Furthermore, there were no significant interactions between factors, meaning that the behaviour of the classification accuracy to the band combination were similar for both images, as reflected in Table 3.

A general analysis of the classification presented in this section indicates that not all classifications behave similarly. On the one hand, the QB classification gave

Table 3

Quality indexes in the image classification of the multi-spectral images

Treatment	BF		MF		GDP		QP	
	QB	IK	QB	IK	QB	IK	QB	IK
1: R, G, B	0.33	0.46	0.032	0.040	96.89	96.12	73.85	66.88
2: R, G, B, NIR	0.23	0.40	0.075	0.091	93.06	91.70	77.21	67.21
3: R, G, B, Pan	0.23	0.38	0.078	0.085	92.76	92.22	76.74	68.58
4: R, G, B, NIR, Pan	0.18	0.36	0.146	0.158	87.30	86.45	76.08	66.38

The values correspond to the mean of five repetitions in each treatment.

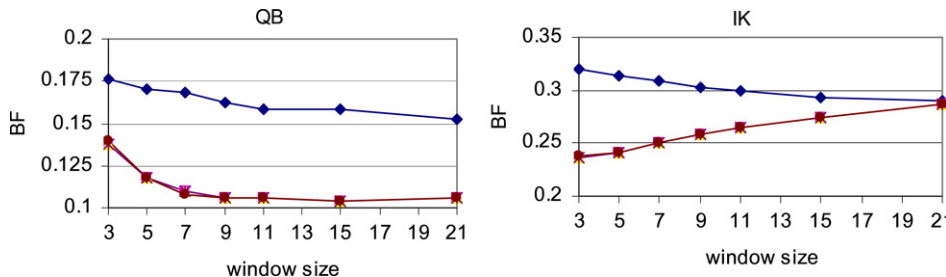


Fig. 3. BF index value for each window size and grey level values used to calculate the MEA texture parameter, for each of the images studied (right: IK image, left: QB image). Grey levels:  $\blacklozenge = 1024$ ,  $\blacksquare = 256$ ,  $\blacktriangle = 128$ ,  $\times = 64$ ,  $\diamond = 32$ ,  $\bullet = 16$ .

better values for the BF and QP indexes than did the IK classification, and on the other hand treatment 1 (RGB band combination) gave the best values of MF and GDP in both images while no significant differences were found between the images for these indexes. Better values of QP in the QB image than in the IK image were not associated with worse values of MF and GDP in the QB image, as shown in Table 3. This contrasts with the results of Lee et al. (2003), who, working with an IK image to detect buildings in urban areas, found an increase in the MF and a decrease in the BDP (Building Detection Percentage), linked to an increase in the QP when different classification methods were used. In the study by Wang et al. (2004), the capability of a QB image and an IK image of the same area was compared in order to detect different mangrove varieties; examining seven land-cover classes, which included some types other than mangrove, the authors found that classification based on the IK image using only multi-spectral bands (equivalent to our treatment 2) was slightly but significantly more accurate than when based on multi-spectral QB imagery. This contrasts with our results since, for this treatment, we found significant differences for BF and QP in favour of the QB image, whereas none were found between images for indexes MF and GDP.

The results from the study by Wang et al. (2004) showed that adding the panchromatic band to the classification (equivalent to our treatment 4) did not significantly improve accuracy with regard to the equivalent of our treatment 2, although the IK image still showed considerably better results. We found that, although neither QP nor BF varied when the panchromatic band was added, MF and GDP did significantly differ in these treatments, with the best values appearing for the treatment in which only multi-spectral bands were taken into account for classification (treatment 2). As in the previous case, our results indicate that the significant differences between images appeared in indexes BF and QP, in both cases in favour

of the QB image. In any case, when these authors focused on the classes corresponding to the mangrove varieties, they found that, in terms of the variety under study, each image differed in the accuracy of the classifications.

#### 4.2. Comparison of classifications based on spectral and texture information

Table 4 presents the ANOVA table of the significance of the image, texture parameter, window size, and grey level, and their interactions on the classification quality indexes. Furthermore, Table 5 shows the average values of the quality indexes for each texture parameter and for each image.

Table 4 indicates that all single factors were highly significant in explaining the overall variation of BF, while two- and three-way interactions were not statistically significant. The LSD test to compare the means of BF by the single factors left indicated that by factor A (image), the QB image showed a significantly lower value than the IK image. By factor B (texture parameter), the MEA parameter showed a significantly lower value than the rest of texture parameters (Table 5). By factor C (window size), only the  $3 \times 3$  showed a worse value than the rest of levels of this factor, which formed a homogeneous group. By factor D (grey level), only the 1024 grey level registered a worse value than the rest of levels, which formed a homogeneous group. The minimum BF value was found in both images for the MEA parameter: 0.104 in QB, with a ws of  $15 \times 15$  and grey levels of 16, 64, 128 and 256; and 0.237 in IK, with a ws of  $3 \times 3$  and grey level of 128. Fig. 3 shows the BF index value for each ws and grey level used to calculate the MEA texture parameter, for each of the images studied.

All single factors were highly significant in explaining the overall variation of MF (Table 4), and the interaction between factors B (texture parameter) and C (window size), and interaction between factors

Table 4

ANOVA table of the significance of the image, texture parameter, window size, and grey level, and their interactions on image-classification accuracy (df: degrees of freedom)

Source	df	Sum of squares	F-values	P-values	Source	df	Sum of squares	F-values	P-values
<b>BF</b>									
Image (A)	1	22.6779	4531.83	<0.001	Image (A)	1	1185.54	271.51	<0.001
Texture parameter (B)	9	2.22443	49.39	<0.001	Texture parameter (B)	9	8280.86	210.72	<0.001
Window size (C)	6	0.20432	6.8	<0.001	Window size (C)	6	1200.28	45.81	<0.001
Grey level (D)	5	0.22969	9.18	<0.001	Grey level (D)	5	577.948	26.47	<0.001
A*B	9	0.02451	0.54	0.8439	A*B	9	1423.15	36.21	<0.001
A*C	6	0.02832	0.94	0.4634	A*C	6	99.8944	3.81	<0.001
A*D	5	0.00125	0.05	0.9973	A*D	5	53.0567	2.43	0.0327
B*C	54	0.21706	0.8	0.848	B*C	54	885.797	3.76	<0.001
B*D	45	0.20862	0.93	0.6129	B*D	45	482.254	2.45	<0.001
C*D	30	0.00951	0.06	1	C*D	30	116.206	0.89	0.6436
A*B*C	54	0.10574	0.39	1	A*B*C	54	274.593	1.16	0.1927
A*B*D	45	0.02231	0.1	1	A*B*D	45	329.315	1.68	0.0033
A*C*D	30	0.00125	0.01	1	A*C*D	30	120.715	0.92	0.5894
B*C*D	270	0.03257	0.02	1	B*C*D	270	452.989	0.38	1
Residual	3630	18.165			Residual	3630	15850.5		
Total	4199	44.1524			Total	4199	31333.1		
<b>MF</b>									
Image (A)	1	0.25061	289.53	<0.001	Image (A)	1	73262.3	6259.03	<0.001
Texture parameter (B)	9	1.62525	208.63	<0.001	Texture parameter (B)	9	3410.31	32.37	<0.001
Window size (C)	6	0.25142	48.41	<0.001	Window size (C)	6	117.837	1.68	0.1212
Grey level (D)	5	0.11295	26.1	<0.001	Grey level (D)	5	138.662	2.37	0.0369
A*B	9	0.30524	39.18	<0.001	A*B	9	894.711	8.49	<0.001
A*C	6	0.01237	2.38	0.0266	A*C	6	24.7449	0.35	0.9088
A*D	5	0.009	2.08	0.0642	A*D	5	41.136	0.7	0.6237
B*C	54	0.1606	3.44	<0.001	B*C	54	799.42	1.26	0.0932
B*D	45	0.10007	2.57	<0.001	B*D	45	600.363	1.14	0.2423
C*D	30	0.00917	0.35	0.9995	C*D	30	80.0735	0.23	1
A*B*C	54	0.04361	0.93	0.6143	A*B*C	54	291.065	0.46	0.9997
A*B*D	45	0.06417	1.65	0.0044	A*B*D	45	250.486	0.48	0.9988
A*C*D	30	0.00961	0.37	0.9993	A*C*D	30	49.1496	0.14	1
B*C*D	270	0.03843	0.16	1	B*C*D	270	437.793	0.14	1
Residual	3630	3.14207			Residual	3630	42489.4		
Total	4199	6.13457			Total	4199	122887		
<b>QP</b>									

Table 5

Quality indexes in the image classification based on spectral and texture information

Text. param.	BF		MF		GDP		QP	
	QB	IK	QB	IK	QB	IK	QB	IK
HOM	0.185	0.332	0.166	0.187	85.82	84.37	74.32	65.86
CON	0.162	0.314	0.201	0.195	83.35	83.70	73.60	66.31
DIS	0.160	0.310	0.216	0.191	82.31	84.01	72.84	66.66
MEA	0.120	0.266	0.176	0.205	85.04	83.05	77.25	68.03
STD	0.157	0.294	0.151	0.186	86.86	84.43	76.66	67.63
ENT	0.184	0.328	0.146	0.170	86.98	85.58	75.76	66.77
ASM	0.204	0.348	0.125	0.147	88.78	87.24	75.62	66.89
COR	0.189	0.345	0.152	0.178	86.82	85.00	74.91	65.69
G-ASM	0.190	0.338	0.147	0.165	87.18	85.96	75.08	66.61
G-ENT	0.179	0.323	0.166	0.178	85.82	85.00	74.64	66.69

The values correspond to the mean of all classifications for each parameter. In each column, the best values obtained by the LSD test ( $p < 0.05$ ), have been shaded.

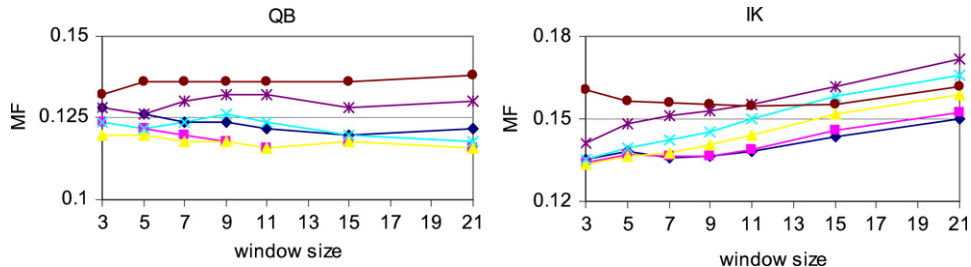


Fig. 4. MF index value for each window size and grey level values used to calculate the ASM texture parameter, for each of the images studied (right: IK image, left: QB image). Grey levels:  $\blacklozenge = 1024$ ,  $\blacksquare = 256$ ,  $\blacktriangle = 128$ ,  $\times = 64$ ,  $\bullet = 16$ .

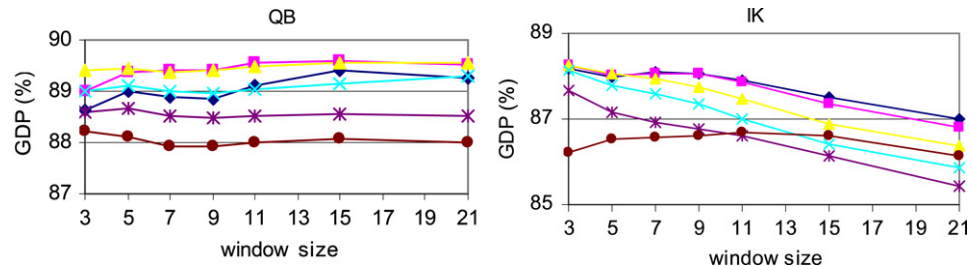


Fig. 5. GDP index value for each window size and grey level values used to calculate the ASM texture parameter, for each of the images studied (right: IK image, left: QB image). Grey levels:  $\blacklozenge = 1024$ ,  $\blacksquare = 256$ ,  $\blacktriangle = 128$ ,  $\times = 64$ ,  $\bullet = 16$ .

B and D (grey level) were also statistically significant. The rest of the two- and three-way interactions were not statistically significant, signifying that the behaviour of the texture parameters was statistically sensitive to the variation of ws and grey level. The LSD test to compare the means of MF by the single factors indicated that by factor A (image), the QB image showed a significantly lower value than did the IK image. By factor B (texture parameter), the ASM parameter showed a significantly lower value than did the rest of texture parameters (Table 5). By factor C (window size), the  $3 \times 3$  and  $15 \times 15$  levels showed the best value. By factor D (grey level), the 128 grey level showed the best value. In both images, the minimum MF value was found in parameter ASM: 0.116 in QB, with ws of  $11 \times 11$  and  $21 \times 21$ , and grey levels of 256 and 128; and 0.134 in IK, with a ws of  $3 \times 3$  and grey level of 128. Fig. 4 shows the MF index value for each ws and grey level used to calculate the ASM texture parameter, for each of the images studied.

In the GDP index, all single factors were highly significant to explain its overall variation (Table 4), and except for the interaction between factors A (image) and D (grey level), and between factors C (window size) and D, the rest of the two-way interactions were significant. The three-way interactions were not statistically significant. The LSD test to compare the means of QP by the single factors revealed that by factor A (image), the QB image had a significantly higher value than the IK image, this difference being considerable, as reflected in Table 5. By factor B (texture parameter), the MEA parameter showed a significantly higher value than the rest of the texture parameters. The best results were given in both images for parameter MEA: 89.608% in QB, for a ws of  $15 \times 15$  and a grey level of

these differences were slight, and even GDP for the IK image was higher in the IK image than in the QB image for CON and DIS texture parameters, as reflected in Table 5. By factor B (texture parameter), the ASM parameter showed a significantly higher value than did the rest of texture parameters (Table 5). By factor C (window size), the  $3 \times 3$  and  $15 \times 15$  levels showed the best values and by factor D (grey level), the 128 and 256 levels gave the best values. The best results were found in both images for parameter ASM: 89.608% in QB, for a ws of  $15 \times 15$  and a grey level of 256; and 88.256% with a ws of  $3 \times 3$  and a grey level of 128 in the IK image. Fig. 5 shows the GDP index value for each ws and grey level used to calculate the ASM texture parameter, for each image studied.

The significant main factors explaining overall variation of the QP index were only A (image) and B (texture parameter), and the interaction between them was also significant (Table 4). The rest of the main factors, two- and three-way interactions were not significant. The LSD test to compare the means of QP by the single factors revealed that by factor A (image), the QB image had a significantly higher value than the IK image, this difference being considerable, as reflected in Table 5. By factor B (texture parameter), the MEA parameter showed a significantly higher value than the rest of the texture parameters. The best results were given in both images for parameter MEA: 89.608% in QB, for a ws of  $15 \times 15$  and a grey level of

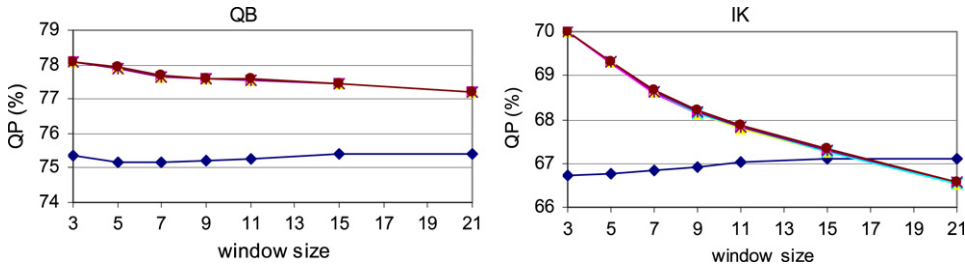


Fig. 6. QP index value for each window size and grey level values used to calculate the MEA texture parameter, for each of the images studied (right: IK image, left: QB image). Grey levels:  $\diamond = 1024$ ,  $\blacksquare = 256$ ,  $\blacktriangle = 128$ ,  $\times = 64$ ,  $\circledast = 32$ ,  $\bullet = 16$ .

256; and 88.256% with a ws of  $3 \times 3$  and a grey level of 128 in the IK image. Fig. 6 shows the QP index value for each ws and grey level used to calculate the MEA texture parameter, for each image studied.

The results analysed in this section up to this point can be compared with those reported by other authors in similar studies. For example, the above-mentioned study by Wang et al. (2004) verified that the capacity for mapping mangrove changed when a band related to the texture of the image was added to the multi-spectral bands of a QB image and an IK image. Their results reveal that when the STD texture parameter was used, there was a significant improvement in the classification in both images, with just a  $21 \times 21$  ws, although there were no significant differences from one image to the other. In all the window sizes studied, the results were better in IK than in QB. Nevertheless, our results show opposite trends between the images: except on two occasions (Table 5), the quality indexes were better in the QB image than in the IK image, and differences were generally significant in favour of the QB image. Also, our results did not show a clear tendency of the influence of the ws, as illustrated in Figs. 3–6. With regard to ws, our results for the parameter STD partially coincide, although a higher QP value was found in the QB image for a ws of  $21 \times 21$ , whereas in IK the maximum value occurred for an  $11 \times 11$  ws, and in neither case were they significantly different from those found with the rest of the ws (data not shown). Whereas in Wang's study the lowest classification accuracy was detected in both images for a ws of  $7 \times 7$  and  $9 \times 9$  in the IK image and in the QB image respectively, the tendency observed in our case varied in each image: in the QB image the QP index increased with the ws, whilst the maximum value in the IK image occurs for an  $11 \times 11$  ws. When texture parameters CON, COR and ENT were used for this study, it was verified that the classification results were worse, a trend noted also in our results. In our work, the texture parameter which yielded the best quality classification indexes differed in behaviour: in the IK image the best indexes were found

for a ws of  $3 \times 3$  (this factor was not significant for the QP index), while for the QB image this trend was not similar, since the best values of BF and GDP were found for a ws of  $15 \times 15$ , the best value of MF for ws values of  $11 \times 11$  and  $21 \times 21$ , and the best value of QP was found for a ws of  $3 \times 3$  (in this case, the ws factor was not statistically significant).

Chen et al. (2004) used a 1 m resolution multi-spectral aerial image (R, G, B) of an urban area, which was degraded to different resolutions (4, 8, 12, 16, 20 and 24 m). The lowest resolution that yielded results was 4 m, with 8 different classes being considered. The classification results that took into account only the multi-spectral bands were compared with those found taking into account a texture band added to the multi-spectral image and different ws while using parameter STD. When the texture band was added, results improved in the classification with lower resolution values (4, 8 and 12 m), for different ws values. These researchers conclude that there is no optimal pixel size or ws, but that these parameters depend on the characteristics of the terrain to be classified. With regard to resolution, our results differ, as the QB image classification was more accurate than was the IK image classification in all cases studied by adding texture information to the multi-spectral image, and, except for the QP index, an optimal ws for the MEA and ASM texture parameters was found, as stated above.

Puissant et al. (2005) compared the effect of adding a texture band (HOM, DIS, ENT and ASM) to the multi-spectral bands (R, G, B), and the ws used to calculate the texture parameter on the classification results of various images with different resolutions (1, 2.5, 5 and 10 m). The classification was focused on 7 different classes, and the results revealed a very slight improvement when the texture band was added to all the images, although the parameter that caused the improvement was not the same one. This does not coincide with the outcomes of our study, where a homogeneous performance of the images was observed when confronted with the same

texture parameter (the best quality index values were found in both images for the same texture parameters), and we did not detect improvement of the classification accuracy when the texture information was added to the multi-spectral image. On the other hand, the resolutions that were most affected when the texture information was added were the 1 and 2.5 m. Another important issue from Puissant et al. (2005) is that the same parameter did not influence all classes in the same way. Thus, for example, the 1 m images, which improved the most, overall, did so at the expense of three classes, making the rest worse.

## 5. Conclusions

In the present study, the utility of the texture analysis has been studied with regard to improving classification by pixel in a rural area, where the classification objective was to detect plastic-cover greenhouses. This study was carried out on a QB and an IK image, which allowed us to compare the capability of these images to detect greenhouses.

Some of the major findings from the experimental results are as follows:

1. When only multi-spectral and panchromatic bands were taken into account for classification, all the quality indexes calculated, except GDP, were better in the QB image than in the IK image, although the difference was not always significant.
2. The inclusion of a band with texture information did not significantly improve the quality index values, in relation to those found when only multi-spectral bands were taken into account (the exception being the BF index, which did improve).
3. The classification quality indexes behaved similarly in both images. The better BF and QP values were found for the MEA texture parameter. Furthermore, the better MF and GDP values were found for the ASM texture parameter. The optimum ws in these texture parameters was  $3 \times 3$  for the IK image, while for the QB image it depended on the quality index studied but the optimum ws was around  $15 \times 15$ . With regard to the grey level, the optimum was 128. Thus, the optimum texture parameter depends on the main objective of the image classification. If the main classification goal is to minimize the pixels wrongly classified (low BF and then high QP), the texture parameter to be used should be the MEA, whereas if the main classification goal is to minimize the unclassified pixels (low MF and then high GDP), the texture parameter to be used should be the ASM.

4. To generalise the results of this study with regard to the utility of the texture parameters for an improved per-pixel classification, it would be desirable to have a set of images from different sensors and to include them in the classification of a greater number of classes.

## Acknowledgements

This study has been possible thanks to the funding exceptionally granted by the Education and Science Council of the Andalusian Government through the Oficinas de Transferencia de Resultados de Investigación de las Universidades Andaluzas (Offices of Transference of Research Outcomes of the Andalusian Universities). This Council also funds the project “Generación, integración y actualización de cartografía digital como soporte de modelos de desarrollo rural sostenible. Propuesta metodológica y aplicación en el Campo de Níjar (Almería)” (Generation, integration and updating of digital cartography as a support for sustainable rural-development models. Methodological proposal and application in the Campo de Níjar, Almería).

## References

- Agüera, F., Aguilar, M.A., Aguilar, F.J., 2006. Detecting greenhouse changes from QB imagery on the Mediterranean Coast. *International Journal of Remote Sensing* 27 (21), 4751–4767.
- Aguilar, M.A., Aguilar, F.J., Sánchez, J.A., Carvajal, F., Agüera, F., 2005. Geometric correction of the QuickBird high resolution panchromatic images. In: Proc. XXII International Cartographic Conference, A Coruña, 9–16 July, 7 p. (on CDROM).
- Al-Khudhairi, D.H.A., Caravaggi, I., Giada, S., 2005. Structural damage assessments from ikonos data using change detection, object-oriented segmentation, and classification techniques. *Photogrammetric Engineering and Remote Sensing* 71 (7), 825–837.
- Anys, H., He, D.C., 1995. Evaluation of textural and multipolarization radar features for crop classification. *IEEE Transactions on Geoscience and Remote Sensing* 33 (5), 1170–1181.
- Chen, D., Stow, D.A., Gong, P., 2004. Examining the effect of spatial resolution and texture window size on classification accuracy: An urban environment case. *International Journal of Remote Sensing* 25 (11), 2177–2192.
- Cushnie, J.L., 1987. The interactive effects of spatial resolution and degree of internal variability within land-cover type on classification accuracies. *International Journal of Remote Sensing* 8 (1), 15–29.
- Franklin, S.E., Wulder, M.A., Lavigne, M.B., 2001. Texture analysis of IKONOS panchromatic data for Douglas-fir forest age class separability in British Columbia. *International Journal of Remote Sensing* 22 (13), 2627–2632.
- Fraser, C.S., Baltsavias, E., Gruen, A., 2002. Processing of Ikonos imagery for submetre 3D positioning and building extraction. *ISPRS Journal of Photogrammetry and Remote Sensing* 56 (3), 177–194.

- Gao, J., 1999. A comparative study on spatial and spectral resolutions of satellite data in mapping mangrove forests. *International Journal of Remote Sensing* 20 (14), 2823–2833.
- Gong, P., Marceau, D.J., Howarth, P.J., 1992. A comparison of spatial feature extraction algorithms for land-use classification with SPOT HRV data. *Remote Sensing of Environment* 40 (2), 137–151.
- Green, E.P., Clark, C.D., Mumby, P.J., Edwards, A.J., Ellis, A.C., 1998. Remote sensing techniques for mangrove mapping. *International Journal of Remote Sensing* 19 (5), 935–956.
- Guindon, B., Zhang, Y., Dillabaugh, C., 2004. Landsat urban mapping based on a combined spectral-spatial methodology. *Remote Sensing of Environment* 92 (2), 218–232.
- Haralick, R.M., Shanmugan, K., Dinstein, I., 1973. Textural features for image classification. *IEEE Transactions on Systems, Man and Cybernetics* 3 (6), 610–621.
- Jin, X., Davis, C.H., 2005. An integrated system for automatic road mapping from high-resolution multi-spectral satellite imagery by information fusion. *Information Fusion* 6 (4), 257–273.
- Kayitakire, F., Hamel, C., Defourny, P., 2006. Retrieving forest structure variables based on image texture analysis and IKONOS-2 imagery. *Remote Sensing of Environment* 102 (3–4), 390–401.
- Kiema, J.B.K., 2002. Texture analysis and data fusion in the extraction of topographic objects from satellite imagery. *International Journal of Remote Sensing* 28 (4), 767–776.
- Lee, D.S., Shan, J., Bethel, J.S., 2003. Class-guided building extraction from ikonos imagery. *Photogrammetric Engineering & Remote Sensing* 69 (2), 143–150.
- McKeown, D.M., 1999. Fusion of HYDICE hyperspectral data with panchromatic imagery for cartographic feature extraction. *IEEE Transactions on Geoscience and Remote Sensing* 37 (3), 1261–1277.
- Mesev, V., 2005. Identification and characterisation of urban building patterns using IKONOS imagery and point-based postal data. *Computers, Environment and Urban Systems* 29 (5), 541–557.
- Nichol, J., Lee, C.M., 2005. Urban vegetation monitoring in Hong Kong using high resolution multispectral images. *International Journal of Remote Sensing* 26 (5), 903–918.
- Parra, S., 2004. Análisis económico de la valoración de residuos agrícolas orgánicos. Aplicación a la evaluación de proyectos alternativos en la agricultura protegida almeriense. Ph.D. Thesis. Universidad de Almería, Spain.
- Puissant, A., Hirsch, J., Weber, C., 2005. The utility of texture analysis to improve per-pixel classification for high to very high spatial resolution imagery. *International Journal of Remote Sensing* 26 (20), 733–745.
- Rao, P.V.N., Sai, M.V.R.S., Sreenivas, K., Rao, M.V.K., Rao, B.R.M., Dwivedi, R.S., Venkataratnam, L., 2002. Textural analysis of IRS-ID panchromatic data for land cover classification. *International Journal of Remote Sensing* 23 (17), 3327–3345.
- Sanjuán, J.F., 2004. Estudio multitemporal sobre la evolución de la superficie invernada en la provincia de Almería por Términos Municipales desde 1984 hasta 2004 mediante teledetección de imágenes thematic mapper de los satélites Landsat V y VII, first ed. I. M. Cuadrado.
- Shaban, M.A., Dikshit, O., 2001. Improvement of classification in urban areas by the use of textural features: The case study of Lucknow City, Uttar Pradesh. *International Journal of Remote Sensing* 22 (4), 565–593.
- Steel, R.G.D., Torrie, J.H., 1980. Principles and Procedures of Statistics. A Biometrical Approach, second ed. McGraw-Hill Inc.
- Van Niel, T.G., McVicar, T.R., Datt, B., 2005. On the relationship between training sample size and data dimensionality: Monte Carlo analysis of broadband multi-temporal classification. *Remote Sensing of Environment* 98 (4), 468–480.
- Wang, L., Sousa, W.P., Gong, P., Biging, S., 2004. Comparison of IKONOS and QuickBird images for mapping mangrove species on the Caribbean coast of Panama. *Remote Sensing of Environment* 91 (3–4), 432–440.
- Weber, C., Ranchin, T., 2003. Extraction of urban features in Strasbourg, France: Comparison of two fusion algorithms for Quickbird MS and Pan data. In: Proc. 2nd GRSS/ISPRS Joint Workshop on Data Fusion and Remote Sensing over Urban Areas, Berlin, Germany, 22–23 May 2003. pp. 206–210.
- Yan, D., Zhao, Z., 2003. Road detection from quickbird fused image using IHS transform and morphology. *International Geoscience and Remote Sensing Symposium* 6, 3967–3969.